Received: 20 February 2020 | Revised: 21 April 2020 | Accepted: 30 April 2020

DOI: 10.1096/fj.202000399R

RESEARCH ARTICLE

THE FASEB JOURNAL

Conserved cysteine dioxidation enhances membrane interaction of human Cl^- intracellular channel 5

Alisa Ferofontov[1] | **Pavla Vankova**[2,3] | **Petr Man**[2] | **Moshe Giladi**[1] | **Yoni Haitin**[1,4]

[1]Department of Physiology and Pharmacology, Sackler School of Medicine, Tel-Aviv University, Tel-Aviv, Israel

[2]Division BioCeV, Institute of Microbiology of the Czech Academy of Sciences, Vestec, Czech Republic

[3]Department of Biochemistry, Faculty of Science, Charles University, Prague, Czech Republic

[4]Sagol School of Neuroscience, Tel Aviv University, Tel Aviv, Israel

Correspondence
Yoni Haitin, Department of Physiology and Pharmacology, Sackler Faculty of Medicine, Tel Aviv University, Tel Aviv, Israel.
Email: yhaitin@tauex.tau.ac.il

Funding information
Israel Science Foundation (ISF), Grant/Award Number: 1721/16; The I-CORE program of the Planning and Budgeting Committee and the Israel Science Foundation, Grant/Award Number: 1772/12; Israel Cancer Research Fund (ICRF), Grant/Award Number: 01214; Israel Cancer Research Fund (ICRF), Grant/Award Number: 19202; The German-Israeli Foundation for Scientific Research and Development (GIF), Grant/Award Number: I-2425-418.13/2016; EC | Horizon 2020 Framework Programme (H2020), Grant/Award Number: 731077; Czech Science Foundation (CSF), Grant/Award Number: 19-16084S; MEYS CZ funds, Grant/Award Number: CZ.1.05/1.1.00/02.0109, LM2015043

Abstract

The human chloride intracellular channel (hCLIC) family is thought to transition between globular and membrane-associated forms by exposure of a hydrophobic surface. However, the molecular identity of this surface, and the triggering events leading to its exposure, remain elusive. Here, by combining biochemical and structural approaches, together with mass spectrometry (MS) analyses, we show that hCLIC5 is inherently flexible. X-ray crystallography revealed the existence of a globular conformation, while small-angle X-ray scattering showed additional elongated forms consisting of exposure of the conserved hydrophobic inter-domain interface to the bulk phase. Tryptophan fluorescence measurements demonstrated that the transition to the membrane-associated form is enhanced by the presence of oxidative environment and lipids. Using MS, we identified a dose-dependent oxidation of a highly conserved cysteine residue, known to play a key role in the structurally related omega-class of glutathione-S-transferases. Hydrogen/deuterium exchange MS analysis revealed that oxidation of this cysteine facilitates the exposure of the conserved hydrophobic inter-domain interface. Together, our results pinpoint an oxidation of a specific cysteine residue as a triggering mechanism initializing the molecular commitment for membrane interaction in the CLIC family.

KEYWORDS

CLIC, mass spectrometry, oligomerization, oxidation, X-ray crystallography

Abbreviations: BFC, BODIPY FL L-Cystine; CLIC, chloride intracellular channel; Cu:Phe, copper-phenanthroline; DSF, differential scanning fluorimetry; DSS, disuccinimidyl suberate; EOM, ensemble optimization method; ESI, electrospray ionization; GST, glutathione-S-transferase; HDX, hydrogen/deuterium exchange; LUV, large unilamellar vesicles; MALS, multi-angle light scattering; MEG, monoethylene glycol; MS, mass; PTM, putative transmembrane region; SAXS, small-angle X-ray scattering; SEC, size-exclusion chromatography; SM, sphingomyelin; TCEP, tris(2-carboxyethyl) phosphine; TEV, tobacco etch virus; TRX, thioredoxin.

1 | INTRODUCTION

The chloride intracellular channel (CLIC) family forms a class of unusual proteins that exhibit both globular and membrane-associated forms.[1] First identified in bovine kidney cortex vesicles and apical membranes of the trachea following indanyl-oxyacetic acid 94-mediated affinity purification, CLIC5 (p64), the founding member of the family, gave rise to distinctive Cl^- ion channel properties during subsequent in vitro reconstitution studies.[2] However, later sequence analysis revealed a weak yet significant homology to the omega-class of glutathione-S-transferases (GST),[3] and the perplexing lack of structural similarity to other families of chloride channels. Indeed, comprehensive structural investigations later revealed a globular organization, reminiscent of the GST-fold, composed of an N-terminal thioredoxin domain (TRX) followed by a C-terminal α domain.[4-9] Finally, while the underlying structural mechanisms remain enigmatic, CLIC family members were shown to alternate between soluble and membrane-bound conformations.[10]

In humans, the CLIC family consists of six isoforms (CLIC1-6).[4-8] While varying in overall lengths, the C-terminal ~220 residues constitute the CLIC homology domain, demonstrating canonical, and highly conserved structural properties. Despite the overwhelming structural similarity between different CLIC isoforms, isoform-specific tissue, and cellular distributions were shown, suggesting a degree of functional specialization is required for various cellular processes involving CLICs.[1] Further supporting this notion, different CLIC isoforms were associated with disease processes involving different tissues.[11-21] While considerable efforts have been directed toward inferring the functional "channel-like" properties of the family from structural analyses of the soluble form, the obligatory protein oligomerization and membrane interaction mechanisms, crucial for channel formation and function, remain confounded.

To date, most of the mechanistic insights concerning the structural transition between the globular and membrane-bound conformations of CLICs arise from studies of the CLIC1 isoform. Using biochemical and spectroscopic approaches, CLIC1 was shown to interact with the membrane in a process involving extensive conformational rearrangements.[22] Importantly, oxidative or acidic environments enhanced this process, suggesting a possible role in the triggering mechanism initiating the structural transformation of CLIC1.[23] Specifically, CLIC1 was shown to undergo an oxidation-mediated exposure of a large hydrophobic surface following the formation of an intra-molecular disulfide bridge.[24] It was suggested that in the presence of membranes this hydrophobic surface promotes membrane interaction, while in solution this surface mediates dimerization.[22] However, one of the involved cysteine residues (C59) is unique to CLIC1, suggesting either an unresolved general mechanism of response to oxidative environment, or a differential isoform-specific mechanism for membrane interaction.

Conversely, our recent studies of the metamorphic nature of CLIC6, using structural and biochemical approaches, highlight the response of CLIC1 to oxidative conditions as unique. Indeed, despite displaying a nearly identical structure in comparison to the soluble monomeric form of CLIC1 (RMSD = 0.5 Å), CLIC6 does not undergo oxidation-dependent dimerization in solution. However, in the presence of membranes, CLIC6 displays significant oligomerization, which is enhanced by an oxidative environment. These results indicate an oxidation-mediated exposure of a hydrophobic surface, raising the possibility for a common mechanism which does not require disulfide bridge formation prior to membrane interaction. Indeed, small-angle X-ray scattering (SAXS) experiments suggested that CLIC6 samples both a globular conformation (as observed in the crystal structures) and an elongated conformation, in which the conserved hydrophobic inter-domain interface is exposed.[8] Interestingly, CLIC1 was also suggested to exhibit an extended conformation in phospholipid bilayer, such that the TRX and α domains can be situated on opposite sides of the membrane.[25]

Here, in order to gain mechanistic insights into the membrane interaction and oxidation response of CLICs, we investigated the founding member of the family, the human CLIC5 (hCLIC5). Importantly, hCLIC5 was associated with human diseases ranging from deafness and renal dysfunction[26,27] to malignancies.[28,29] Using a multifaceted biochemical and structural approach, together with MS analyses, we show that hCLIC5, similarly to CLIC6, is inherently flexible. Furthermore, while hCLIC5 undergoes oxidation-dependent oligomerization in solution, this property is not a prerequisite for membrane interaction. Instead, this membrane interaction is enhanced by the specific oxidation of a highly conserved cysteine residue and is crucial for interaction with the membrane.

2 | MATERIALS AND METHODS

2.1 | Overexpression and purification of hCLIC5

Human CLIC5 (isoform B; Genebank accession code AAF66928.1) CLIC domain (residues 16-251; termed hCLIC5) was sub-cloned using 5′ NcoI and 3′ HindIII sites into a pETM11 vector containing an N-terminal hexa-histidine affinity tag followed by a tobacco etch virus protease (TEV) cleavage site. The mouse CLIC6 (mCLIC6) used was previously described.[8] C32S, C165S, C186S, and C231S (hCLIC5) and S512C (mCLIC6) were introduced using the standard QuickChange approach. Constructs had a GAMG cloning artifact sequence introduced at their amino terminus and were verified by sequencing. hCLIC5 (WT and mutants) were expressed

in T7 Express *Escherichia coli* cells (New England Biolabs) as previously described.[8] Bacterial cultures were grown to mid-log phase in terrific broth (Formedium) and induced with 0.25 mmol/L isopropyl β-D-1-thiogalactopyranoside (Formedium) overnight at 16°C. Cells were harvested and re-suspended in 250 mmol/L NaCl, 50 mmol/L Tris-HCl (pH 8.0)and 1 mmol/L tris(2-carboxyethyl)phosphine (TCEP) (buffer A), supplemented with 15 mmol/L imidazole and containing 2.5 μg mL^{-1} DNaseI, 5 mmol/L $MgCl_2$, 10 mg lysozyme (Fisher Scientific), 1 mmol/L phenylmethane sulfonyl fluoride, and Protease Inhibitor Cocktail Set III (Sigma-Aldrich). Cells were lysed with an EmulsiFlex C-3 homogenizer (Avestin) and the lysate was cleared by centrifugation at 40,000 *g* for 45 minutes at 4°C. hCLIC5 was then loaded onto a Ni^{2+} affinity resin column (HisTrap HP; GE Healthcare), followed by a wash step with buffer A containing 27 mmol/L imidazole and eluted using buffer A supplemented with 300 mmol/L imidazole. The hexa-histidine tag was removed by TEV cleavage overnight at 4°C. Imidazole was removed using a HiPrep 26/10 desalting column (GE Healthcare) equilibrated with buffer A with 15 mmol/L imidazole. The cleaved protein was loaded onto a second Ni^{2+} column with 15 mmol/L imidazole to remove the cleaved hexa-histidine tag and TEV protease. The flow-through was collected, concentrated to 4-5 mL, and loaded onto a HiLoad 16/60 Superdex 75 column (GE Healthcare) equilibrated with gel filtration buffer, containing 150 mmol/L NaCl and 20 mmol/L Na^+-HEPES (pH7.5). Finally, pooled fractions were concentrated to ~200-800 μmol/L, depending on downstream experiments, using a 10-kDa molecular weight cut-off concentrator (Millipore), flash-frozen in liquid N_2 and stored at −80°C until use.

2.2 | Size exclusion chromatography multi-angle light scattering

Experiments were performed with a preequilibrated analytical SEC column (Superdex 200 Increase 10/300 GL; GE Healthcare) equilibrated with gel filtration buffer. Samples of WT or mutant hCLIC5 (50 μL, 74 μmol/L), naïve or following treatment with 100 μmol/L copper-phenanthroline (Cu:Phe) were loaded onto an HPLC column connected to an 8-angle light scattering detector, followed by a differential refractive-index detector (Wyatt Technology). Refractive index and MALS readings were analyzed with the Astra software package (Wyatt Technology) to determine molecular mass.

2.3 | Cross-linking oligomerization analysis

About 8 μmol/L of hCLIC5 were pre-incubated with 0-400 μg of large unilamellar vesicles (LUV) in the presence or absence of 2 mmol H_2O_2 at 4°C for 2 hours in binding buffer, containing 150 mmol/L NaCl and 20 mmol/L Na^+-HEPES (pH 7.5). Next, cross-linking was performed using 1 mmol/L disuccinimidyl suberate (DSS; Life Technologies) at 4°C for 1 hour. Reactions were quenched by the addition of sodium dodecyl sulfate- and β-mercaptoethanol-containing sample buffer, followed by 10 minutes incubation at room temperature. Cross-linked products were analyzed by SDS-PAGE.

2.4 | Kinetic tryptophan fluorescence measurements

About 10 mg of chloroform dissolved *E. coli* Total lipid Extract (Avanti Polar Lipids), were dried under high vacuum for 1 hour, followed by rehydration with 1.1 mL of assay buffer containing 150 mmol/L NaCl, 1 mmol/L EDTA, and 50 mmol/L Na_3PO4 (pH 6.0). An ultrasonic bath was used to produce multilamellar vesicles, which were further extruded using a 0.2 μmol/L membrane to generate LUV. Experiments were carried out in a 100 μL of reaction final volume, containing 20 μmol/L hCLIC5 in the assay buffer, in presence or absence of 830 μg LUV or 2 mmol/L H_2O_2 (n = 5-6). Fluorescence kinetics were performed using a SpectraMax M5 plate reader (Molecular Devices), using 290 nm and 340 nm excitation and emission wavelengths, respectively, and are presented as F/F_0.

2.5 | Protein crystallization and data collection

Crystals of hCLIC5 were grown at 19°C using hanging-drop vapor diffusion by mixing a 1:1 ratio (v/v; Mosquito, TTP Labtech) of protein solution at 475 μmol/L and a reservoir solution, containing 15%-18% (w/v) PEG 3350, 0.1 mol/L NaSCN, supplemented with 3%-13% (v/v) monoethylene glycol (MEG). This condition produced crystals within 1 day, which grew to maximum size of about 200 × 100 × 100 μm after 7 days. For diffraction data collection, crystals were immersed in liquid N_2 after cryoprotection with 20% MEG. Data were collected at 100 K on beamline ID30B of the European Synchrotron Radiation Facility (ESRF), using a wavelength of 0.976 Å. Integration, scaling and merging of the diffraction data were done with the XDS program.[30] The crystals belonged to space group C 1 2 1 (a = 130.9 Å, b = 93.8 Å and c = 109.5 Å with α = γ = 90° and β = 124.1°). As both datasets were anisotropic, an ellipsoidal truncation and anisotropic scaling were performed[31] using resolution cutoffs of a* = 2.4 Å, b* = 2.1 Å, c* = 2.3 Å.

2.6 | Structure determination

The structure was solved by molecular replacement using the programs PHASER[32] and PHENIX[33] with the structure of the soluble form of mCLIC6 (PDB accession 6ERZ) as the search model. Data collection and refinement statistics are summarized in Table 1. Each asymmetric unit contained four protein chains. Iterative model building and refinement were carried out in PHENIX with manual adjustments using COOT.[34] All structural illustrations were prepared with UCSF Chimera (https://www.cgl.ucsf.edu/chimera).

2.7 | Small-angle X-ray scattering data collection and analysis

Small-angle X-ray scattering data were measured at beamline BM29 of the European Synchrotron Radiation Facility (ESRF), Grenoble, France. Data were collected at 5°C with X-ray beam at wavelength λ = 1.0 Å, and the distance from the sample to detector (PILATUS 1 mol/L, Dectris Ltd, Baden, Switzerland) was 2.867 meters, covering a scattering vector range ($q = 4\pi\sin\theta/\lambda$) from 0.0025 to 0.5 $Å^{-1}$. 10 frames of two-dimensional images were recorded for each buffer or sample, with an exposure time of 1 second per frame. The 2D images were reduced to one-dimensional scattering profiles and the scattering of the buffer was subtracted from the sample profile using the software on site. Samples were analyzed in gel filtration buffer. To account for possible inter-particle effects, each sample was measured at three concentrations (Table 2). The lowest concentration curve was merged with a higher concentration curve at $q \sim 0.2$ $Å^{-1}$ to prevent distortion of the low-angle data, while preserving high signal-to-noise ratio at the higher angles, which are far less sensitive to interparticle effects.[35] The experimental radius of gyration (Rg) was calculated from data at low q values in the range of $qRg < 1.3$, according to the Guinier approximation: $\ln I(q) \approx \ln(I(0)) - Rg^2q^2/3$ using PRIMUS.[36] The D_{max} values and the Porod volume were derived from the paired-distance distribution function (PDDF or $P(r)$) calculated using GNOM.[37] The solution scattering of the crystal structure was calculated using CRYSOL.[38] Missing loops from the crystal structure were generated using MODELLER[39] and the solution scattering of the model was calculated using CRYSOL.[38]

TABLE 1 Crystallographic statistics

Data collection	
Space group	C1 2 1
Cell dimensions	
a, b, c (Å)	130.9, 93.8, 109.5
α, β, γ (°)	90.0, 124.1, 90.0
Beamline	ESRF ID30B
Wavelength (Å)	0.976
Resolution (Å)	2.09
Multiplicity	3.00
Completeness (%)	97.1
Mean I/σ (I)	6.62
R_{merge} (%)	11.1
Refinement statistics	
No. reflections (work/free)	46773/2494
Resolution range[a]	46.81-2.15
R_{work}/R_{free}	0.2015/0.2447
No. atoms	
Macromolecules	6545
Ligands	39
Solvent	381
Average *B*-factor	
Macromolecules	48.26
Ligands	63.70
Solvent	48.80
RMSD (bond lengths)	0.006
RMSD (bond angles)	1.17
Ramachandran outliers (%)	0

[a]After anisotropic scaling.

2.8 | Ensemble optimization method (EOM) analysis

A pool of 10,000 stereochemically feasible structures with a random linker between the TRX and α-domains were generated using the software RANCH.[40] Next, GAJOE,[40] a program that selects an ensemble with the best fit to the experimental data using a genetic algorithm, used this pool as an input. Briefly, 50 ensembles of 20 orientations each were "crossed" and "mutated" for 1,000 generations and the process was repeated 50 times.

2.9 | BODIPY FL L-Cystine (BFC) differential scanning fluorimetry (DSF)

About 10 μmol/L hCLIC5 WT or C165S were pre-incubated with 1 mmol/L DSS or 2% DMSO for 2 hours at 4°C, following by quenching the reactions using the addition of 50 mmol/L TRIS (pH 8). Next, equal volumes of the reactions and a stock of the cysteine reactive fluorescent dye BFC (Life Technologies) were mixed so final concentrations of 5 μmol/L protein and 12 μmol/L dye were reached. Final mixture contained 150 mmol/L NaCl, 20 mmol/L Na^+-HEPES (pH 7.5), and 1% DMSO buffer in 20 μL. Finally,

TABLE 2 SAXS data collection and scattering-derived parameters

Data collection parameters		
Sample	WT	C165S
Beamline	ESRF BM29	
Beam geometry (mm^2)	0.7 × 0.7	
Wavelength (Å)	1.0	
Q range ($Å^{-1}$)	0.0025-0.5	
No. of frames	10	10
Exposure per frame (seconds)	1	0.5
Concentration (mg/mL)	6.5, 3.2, 2.1	3.8, 2, 0.8
Temperature (°C)	5	
Structural parameters		
R_g (Å) [from $P(r)$][a]	21.6 ± 0.002	21.7 ± 0.005
R_g (Å) (from Guinier)[a]	21.5 ± 0.1	21.4 ± 0.1
D_{max} (Å)[b]	70 ± 7	70 ± 7
Porod volume (10^3 $Å^3$)	38.62	38.53
χ^2 CRYSOL	7.9	
χ^2 EOM	0.69	0.79
Software employed		
Primary data reduction	AUTOMAR	
Data processing	PRIMUS	
Modelling	EOM	

[a]±SE.

[b]±10% (estimated range).

DSF assays were performed in a real-time PCR system (n = 6) (QuantStudio 3, Life Technologies), using the ROX filter set in clear 96-well plate.[41] For melting temperature determination, the temperature was increased using a continuous ramp at a rate of 1°C/minute from 4°C to 95°C. Melting temperatures were extracted by Boltzmann sigmoidal fitting of the ascending phase of the curves. For the kinetics measurements, fluorescence was monitored over 12 hours at 25°C.

2.10 | MS and hydrogen/deuterium exchange (HDX)

Two separate HDX experiments with hCLIC5-WT and -C165S were done. One compared WT and C165S forms of hCLIC5 and the other followed hCLIC5-C165S after oxidation by 0.2 and 2 mmol/L H_2O_2. Oxidized samples were prepared by incubating the protein with 0.2 and 2 mmol/L hydrogen peroxide for 10 minutes at 0°C, followed by a gel filtration/buffer exchange. HDX was initiated by a 10-fold dilution of the protein into a D_2O-based buffer, containing 150 mmol/L NaCl and 20 mmol/L Na^+-HEPES (pH7.5), and aliquots were collected after 20 seconds, 2 minutes, 20 minutes, and 2 hours. Exchange was quenched by mixing the sample with equal volume of 0.5 mol/L glycine-HCl buffer (pH 2.3) and rapid freezing in a liquid nitrogen. Next, each sample was thawed and injected on an LC system consisting of immobilized pepsin column, trap column (ACQUITY UPLC BEH C18, 130 Å, 1.7 µm, 2.1 mm × 5 mm, Waters) and an analytical column (ACQUITY UPLC BEH C18, 130 Å, 1.7 µm, 1 mm × 100 mm, Waters). Protein was digested and desalted by 0.4% formic acid (FA) in water for 3 minutes. Solvent was delivered by 1260 Infinity II Quartenary Pump (Agilent Technologies) under flow rate 100 µL/min. Desalted peptides were then eluted and separated on an analytical reversed phase column by water-acetonitrile (ACN) gradient 10%-45% B (solvent A: 0.1% FA in water, solvent B: 0.1% FA/2% water in ACN) pumped by 1290 Infinity II LC system (Agilent Technologies) at 40 µL/min within 7 minutes. The whole setup was cooled down to 0°C to minimize deuterium loss. The LC system was directly connected to an ESI FT-ICR MS (15T solariX XR, Bruker Daltonics) operating in positive MS mode. Acquired data were exported in DataAnalysis 5.0 (Bruker Daltonics,) and processed using in-house developed software DeutEx.[42] Each sample in the WT/C165S comparison experiments was repeated at least in twice, and fully deuterated samples were prepared and analyzed to perform back-exchange correction.[43] Experiments with the oxidized C165S hCLIC5 variant were performed in duplicates at 20 seconds and 20 minutes time points. Data visualization was done using MSTools[44] and PyMOL.

Identification of the peptides generated by online pepsin digestion was achieved through a separated LC-MS/MS analysis using the LC and MS systems and settings as described

above. The MS was at this point operated in data-dependent mode and the resulting MS/MS data were searched using MASCOT (Matrix Science) against a database containing hCLIC5 and pepsin sequences. Search routines as described previously were applied.[45]

Hydrogen peroxide-induced modifications of hCLIC5-WT and -C165S were detected by intact mass measurement. Briefly, the proteins in gel filtration buffer, containing 150 mmol/L NaCl and 20 mmol/L Na^+-HEPES (pH7.5), were incubated with 0, 0.2, 2, 5, and 10 mmol/L H_2O_2 for 10 minutes on ice and then mixed with 10 mmol/L N-acetyl-methionine to quench the reaction. Next, the proteins were reduced with 10 mmol/L TCEP for 10 minutes and immediately desalted using protein OptiTrap (Optimize Technologies). Desalted samples were analyzed via direct infusion on ESI-FT-ICR MS (15T solariX XR, Bruker Daltonics) operating in broad band mode. Resulting electrospray ionization mass spectrometry (ESI-MS) spectra were deconvoluted in DataAnalysis. Localization of the modification site(s) was done by LC-MS/MS analyses as described above. Here, the data were searched using PEAKS X (Bioinformatics Solutions, Waterloo, ON, Canada) to pinpoint possible modifications and the searches were then re-run using MASCOT with single and double oxidation of M, W, Y, C, and F set as variable modification.

3 | RESULTS

3.1 | hCLIC5 undergoes intermolecular disulfide bridge-mediated oligomerization in solution

Chloride intracellular channel 1 was shown to undergo a reversible oxidation-mediated transition between monomeric and non-covalent dimeric states in solution.[24] This dimerization, resulting from extensive conformational changes enabled by an intra-subunit disulfide bond formation and including exposure of a large hydrophobic surface, was suggested to contribute to membrane insertion.[22] However, sequence alignment of the human CLIC isoforms revealed that, while the CLIC1-C24 (C32 in hCLIC5; Figure 1A) is strictly conserved, its counterpart of the oxidation-mediated disulfide bridge formation (C59) is unique to CLIC1 and is replaced with alanine in all other CLIC family members (Figure S1).

In order to discern whether disulfide bridge formation affects hCLIC5 oligomeric state, we first sought to characterize the effect of Cu:Phe on hCLIC5 in solution. Cu:Phe facilitates the formation of disulfide bridges between neighboring cysteine residues. Furthermore, unlike hydrogen peroxide (H_2O_2), Cu:Phe can be easily quenched using EDTA, thus enabling well-controlled incubation periods. Despite the lack of conservation of CLIC1-C59, size exclusion chromatography multi-angle light scattering (SEC-MALS) analysis revealed that while hCLIC5-wild type (WT) forms stable monomers in solution, exposure to 100 µmol/L Cu:Phe resulted in the formation of high-order oligomeric species, with dimers abundance largest following 10 minute incubation (Figure 1B).

Next, in order to determine whether a specific disulfide bridge formation contributes to the oligomerization in solution, we have systematically replaced the four cysteines present in hCLIC5 with a serine residue. While hCLIC5-C32S, -C186S, and -C231S exhibited similar response to oxidative conditions as hCLIC5-WT (Figure S2), the emergence of high-order oligomeric species was completely abolished by the C165S mutation (Figure 1B). This is in line with lack of oxidation-mediated oligomerization of mCLIC6,[8] where this position is naturally substituted with serine (S512; Figure S1), mimicking hCLIC5-C165S. Indeed, mCLIC6-WT demonstrated no oxidation-mediated reactivity (Figure 1C). Strikingly, introducing a

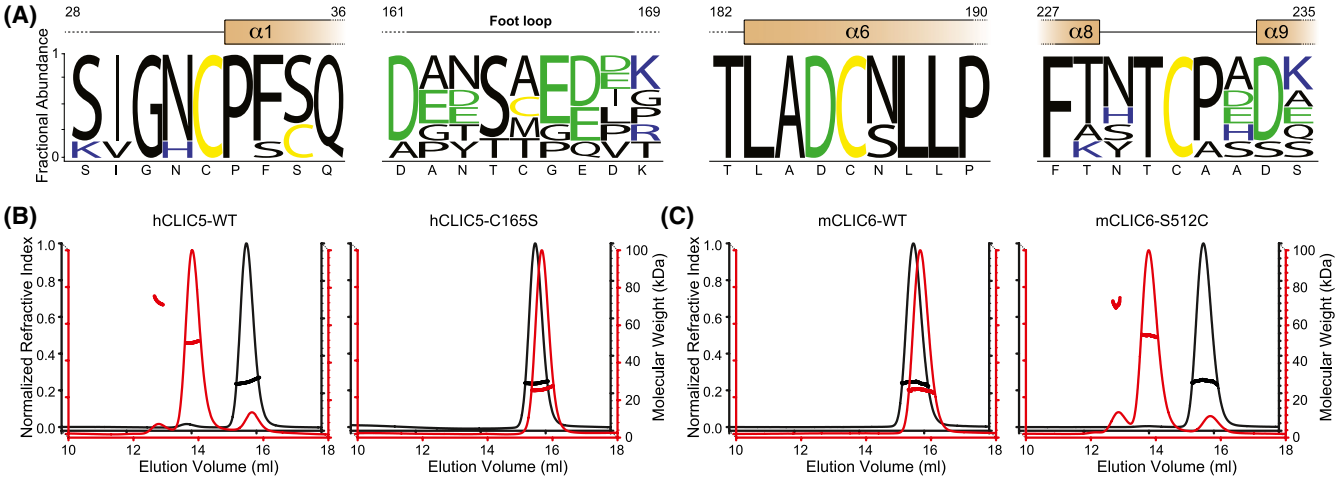

FIGURE 1 C165 mediates hCLIC5 dimerization in the presence of Cu:Phe. A, Logo plots of residues fractional abundance in human CLICs. Shown above are protein regions flanking the four endogenous cysteines of hCLIC5, with secondary structure assignment and hCLIC5 sequence arranged above and below the plots, respectively. B, SEC-MALS analysis of the indicated hCLIC5 mutants (74 µmol/L) in the absence (black) or presence (red) of pre-treatment with 100 µmol/L Cu:Phe. C, Identical analysis as in (B) of mCLIC6-WT and the S512C mutant

cysteine to the homologous position of mCLIC6 (S512C) resulted in oligomerization following exposure to Cu:Phe, similar to hCLIC5 (Figure 1C). Thus, the dependence on a single cysteine residue suggests that initial dimers formation is mediated by a homotypic inter-subunit disulfide bridge formation between C165 residues, rather than non-covalent dimerization resulting from an intra-subunit bridge formation.

3.2 | hCLIC5 oxidation-mediated oligomerization in solution is not required for membrane interaction

It was previously shown that CLICs interact with membranes and that this interaction is facilitated by oxidative conditions.[22,46,47] Interestingly, this feature is shared by CLIC1 and CLIC6, despite their different ability to oligomerize in response to oxidation in solution.[8] Thus, in order to determine the contribution of oxidation-mediated oligomerization to membrane association, we used a cross-linking approach to expose the oligomeric state of hCLIC5, in the presence or absence of H_2O_2 and membranes. Specifically, following incubation of hCLIC5-WT with increasing concentrations of LUV or 2 mmol/L H_2O_2, in the presence of the amine reactive homobifunctional cross-linker DSS, SDS-PAGE analysis revealed distinct high molecular weight bands corresponding mainly to dimers (Figure 2A). Importantly, incubation with both LUV and H_2O_2 resulted in more pronounced oligomerization (Figure 2A). Next, in order to track the time-course and extent of hCLIC5

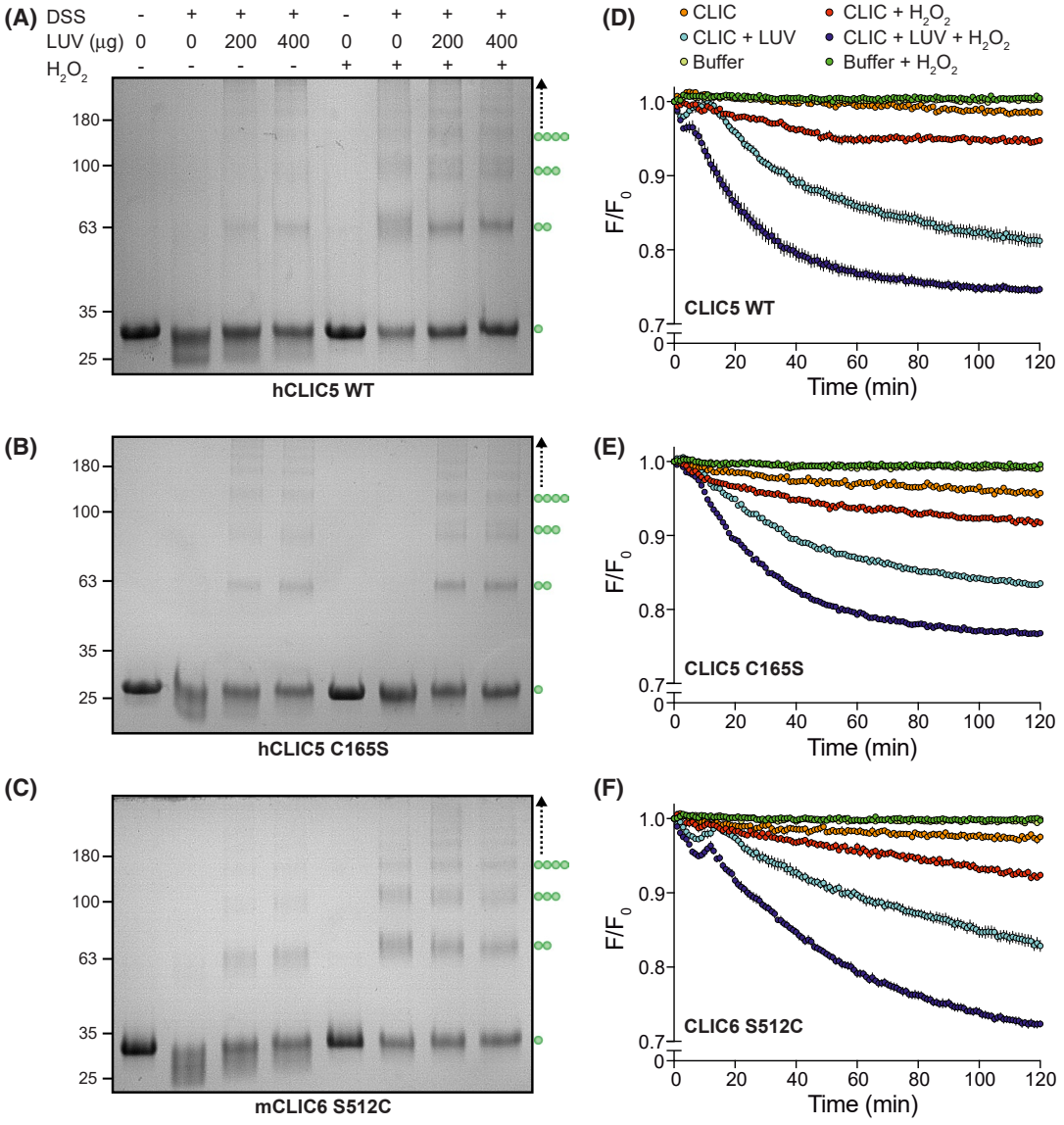

FIGURE 2 Cross-linking and fluorescence analyses of hCLIC5 oligomerization and membrane association. A-C, SDS-PAGE of hCLIC5-WT (A), hCLIC5-C165S (B), and mCLIC6-S512C (C), following DSS-mediated cross-linking in the absence or presence of H_2O_2 and LUV. Green circles represent identified oligomeric states of the protein (n = 3). D-F, Time-dependent tryptophan fluorescence of hCLIC5-WT (D), hCLIC5-C165S (E), and mCLIC6-S512C (F), in the absence or presence of H_2O_2 and LUV, as indicated

interaction with the membrane, we monitored tryptophan fluorescence, which is a commonly used reporter of changes to the local environment of the residue[48] (Figure 2D). hCLIC5 contains two tryptophan residues, W43 and W215 (Figure S1). While under naïve conditions the fluorescence of hCLIC5 remained constant over time, exposure to H_2O_2 led to a small fluorescence reduction following incubation for 2 hours at 25°C (5.2 ± 0.4%), indicating a mild change to the local environment of the tryptophan residues. In contrast, exposure to LUV resulted in a more profound fluorescence decrease (18.8 ± 0.9%), which was further enhanced by adding H_2O_2 (25.3 ± 0.5%). Thus, while H_2O_2 enhances the membrane interaction of hCLIC5, it is not essential for eliciting this process.

Next, in order to discern whether the disulfide bridge formation-mediated oligomerization in solution is involved in membrane association, we examined the ability of hCLIC5-C165S to oligomerize in the presence of LUV. Importantly, while failing to demonstrate DSS-mediated cross-linking in response to H_2O_2, incubation of hCLIC5-C165S with increasing concentrations of LUV resulted in the emergence of high molecular weight species, similar to hCLIC5-WT (Figure 2B). Furthermore, fluorescence kinetics measurements of hCLIC5-C165S accordingly revealed a quenching profile reminiscent of hCLIC5-WT. Intriguingly, while recalcitrant to oxidation-dependent oligomerization, hCLIC5-C165S produced a small fluorescence decrease in the presence of H_2O_2 without LUV (8.3 ± 0.2%), indicating that the mild change to the local environment of the tryptophan residues observed in hCLIC5-WT does not stem from oligomerization. Addition of LUV resulted in a marked fluorescence decrease (16.5 ± 0.2%) which was enhanced by incubation with H_2O_2 (23.2 ± 0.3%) (Figure 2E). Thus, oxidation facilitates membrane interaction in a mechanism independent from oligomerization in solution (Figure 2E).

Finally, we tested the effect of S512C, corresponding to position C165 of hCLIC5 (Figure 1), on the membrane association profile of mCLIC6. We have previously shown, using cross-linking, that mCLIC6-WT behaves like hCLIC5-C165S.[8] Similar to the SEC-MALS analysis of its disulfide bridge-mediated oligomerization, introduction of the S512C mutation resulted in a complete recapitulation of both cross-linking and fluorescence profiles observed in hCLIC5-WT (Figure 2C,F). Specifically, S512C resulted in H_2O_2-dependent emergence of high molecular weight bands, which was enhanced in the presence of LUV (Figure 2C). Furthermore, as in hCLIC5-WT, H_2O_2 resulted in minor tryptophan fluorescence quenching (7.6 ± 0.4%) compared with LUV alone (17.1 ± 0.8%) or in combination with H_2O_2 (27.6 ± 0.4%) (Figure 2F). Thus, the S512C mutation reiterates the significance of the C165 (Figure S1) for oligomerization of hCLIC5 in solution with no apparent effect on the membrane association profile of CLICs.

3.3 | Structural characterization of hCLIC5

Our cross-linking and fluorescence measurements (Figure 2) revealed that hCLIC5 exhibits an intrinsic capacity to interact with membranes, a property which is enhanced by an oxidative environment. These results suggest that hCLIC5 may sample multiple conformations at steady-state, and that oxidation skews the conformational distribution to favor membrane interactions. Thus, in order to uncover the underlying molecular mechanisms, we proceeded with structure analysis of the canonical CLIC domain of hCLIC5. First, we used X-ray crystallography to determine the high-resolution structure of hCLIC5 (Figure 3A; Table 1). The asymmetric unit consisted of four nearly identical chains (average RMSD = 0.39 Å), arranged as two pairs of dimers (Figure S3). However, further analysis of the inter-subunit interface within each dimer revealed a small buried surface area (~540 $Å^2$), suggesting this spatial organization is related to the crystallization process itself. Similar to other CLIC structures, each hCLIC5 subunit occupies ~55 × 54 × 26 $Å^3$ and can be subdivided into a TRX (residues 16-95) and an α (residues 109-248) domains, connected by a short inter-domain linker region (residues 96-108) (Figure 3A). The distinctive TRX and α domains interact via an inter-domain interface, consisting of ~954 $Å^2$ buried surface area (Figure 3B). Except for a single hydrogen bond (Q36-T230), this interface is formed mainly through a network of hydrophobic interactions involving the α1 helix, previously identified as the putative-transmembrane (PTM) region of the family,[4,49,50] and helices α6, α8, and α9 of the α helical domain. The 'foot loop', harboring C165 in hCLIC5, is a long coil between helices α5 and α6 (Figure 1A; Figure S1), found in all CLICs. In the structure of hCLIC5, the "foot loop" is poorly resolved, probably due to a high degree of flexibility in this region. Nevertheless, with C165 crucial for oxidation-mediated dimerization of hCLIC5 (Figure 1B), the structure clearly indicates its high accessibility to the surrounding solution, suggesting that hCLIC5 dimers are formed between two flexible and solvent exposed "foot loops."

Previously, we showed that mCLIC6 samples multiple conformations in solution,[8] possibly exposing its hydrophobic inter-domain interface, using an EOM analysis of SAXS data collected under naïve conditions.[40] Thus, in order to discern whether hCLIC5 shares a similar structural flexibility, we used SAXS to study its properties in solution. First, to assess the agreement between the crystallographic structure and solution data, we employed CRYSOL,[38] which enables the translation of crystal structure coordinates to solution scattering for fitting with an experimental SAXS data. Intriguingly, the structure of hCLIC5 poorly matches the observed solution scattering curve, with $\chi^2 = 7.9$ (Figure 3C). Hence, to ascertain whether hCLIC5 exhibits additional conformations in solution, not sampled by its crystal structure, we used the EOM analysis to obtain a full conformational distribution.[8]

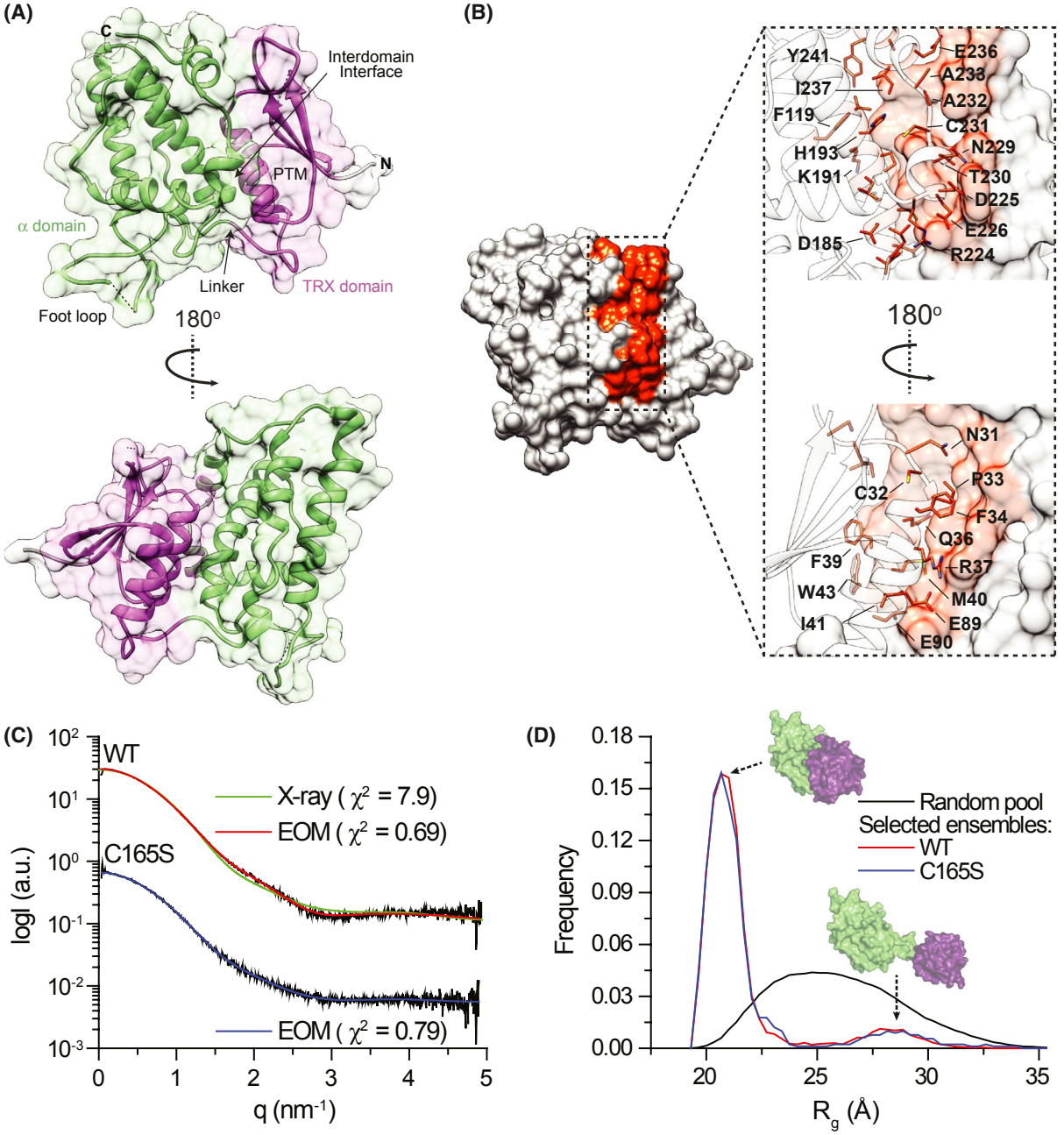

FIGURE 3 Crystal structure and solution properties of hCLIC5. A, Cartoon representation of chain C of hCLIC5 structure. TRX and α domains are indicated, as well as CLIC-specific structural motifs. PTM, putative transmembrane region. B, Surface representation of the inter-domain interface (orange). Residues participating in interface formation are indicated. C, Experimental 2D SAXS curve of hCLIC5 (WT or C165S; black lines) were fit using CRYSOL (green) or EOM (as indicated). D, Random R_g pool (black line) and EOM-selected ensemble distributions of hCLIC5-WT (red line) and -C165S (blue line). Surface representation of highest abundance conformers (R_g = 21.21 Å, 38.3%; R_g = 26.84 Å, 12.1%) is provided

Strikingly, the selected ensemble demonstrates good agreement with the scattering data ($\chi^2 = 0.69$; Figure 3C, Table 2) and shows that, while the crystallized conformation is predominantly frequent in solution (Figure 3D), additional elongated conformations co-exist (Figure 3D). Therefore hCLIC5, as mCLIC6, demonstrates inherent flexibility. Importantly, compared with hCLIC5-WT, SAXS measurements and EOM analysis of C165S, the dimerization resistant mutant of hCLIC5 (Figure 1B), resulted in nearly identical conformational distribution, with a very good agreement between data and fit ($\chi^2 = 0.79$; Figure 3C,D). Together with our previous analysis of mCLIC6, these results suggest that spontaneous exposure of the conserved hydrophobic inter-domain interface (Figure S4)[51] is sufficient for promoting membrane interaction, explaining the oxidation-independent interaction with LUV.

3.4 | hCLIC5 oxidation facilitates exposure of the inter-domain interface

While membrane interaction of CLICs can occur even without oxidative conditions, our tryptophan fluorescence (Figure 2), as well as previous fluorescence resonance energy transfer FRET measurements,[8,46,52] indicate that oxidative environment facilitates the association between CLICs and the membrane. The SAXS data (Figure 3) suggest that this process may be triggered by conformational changes leading to enhanced exposure of the inter-domain hydrophobic interface. However, the EOM analysis a priori presumes that the observed flexibility stems from the inter-domain interface. That is, while our model fits well with the data, it is not necessarily a unique solution.[53] In order to experimentally validate the EOM analysis, we sought an independent method to determine the exposure of the inter-domain interface to bulk phase. hCLIC5 harbors four cysteine residues (Figure 4A), three of which localize to the inter-domain interface, except C165. Thus, by comparing the WT and C165S mutant, the accessibility of the interfacial cysteines in solution was assessed by their site-directed covalent labeling with the BODIPY FL L-cystine (BFC) fluorescent probe. BFC belongs to the class of thiol-reactive probes, which is virtually non-fluorescent in its initial dimeric state.[41] However, upon interaction with protein thiol groups, it undergoes unquenching, giving rise to fluorescence increase which allows monitoring of cysteine labeling. Using differential scanning fluorimetry, we assessed hCLIC5 interface exposure as a function of temperature, either in their native form or following preincubation with the DSS cross-linker. Importantly, exposure to DSS in the absence of LUV and H_2O_2 results in the formation of an auto-crosslinked monomeric population, represented by the appearance of highly mobile species in the SDS-PAGE analysis (Figure 2).

First, we assessed the effect of the C165S mutation on cysteines exposure. hCLIC5-WT and hCLIC5-C165S share an identical melting temperature of 46.4 ± 0.1°C (Figure 4B). Importantly, the amplitude of the temperature-dependent fluorescence change is proportional to the number of cysteine residues in each construct. Moreover, preincubation of hCLIC5-WT and hCLIC5-C165S with 1 mmol/L DSS resulted in a marked shift of the melting temperature to 50.3 ± 0.1°C and 51.6 ± 0.3°C, respectively, and a decrease in the fluorescence signal to a comparable level. Second, kinetics measurements, performed at 25°C over a 12 hour period (Figure 4C), demonstrated that DSS induced a similar decrease of the steady-state BFC fluorescence in both WT and C165S (64.6 ± 1.0% and 59.4 ± 0.8, respectively, n = 6, $P < .01$). Together, these results suggest that DSS auto-crosslinking prevents the exposure of one of the interfacial cysteines to the bulk phase. Indeed, C186 is the only cysteine that is buried within the interface (Figure 4A). This result supports the notions that an extended conformation exists in solution, exposing the inter-domain interface.

In order to directly explore the dynamics and solvent accessibility of the interface between the TRX and α domains, we resorted to use of HDX-MS, monitoring the exchange of backbone amide hydrogens with deuterium, a process which depends on their involvement in secondary structure formation and solvent accessibility.[54] The exchange reaction is quenched at different time points, followed by proteolytic digestion, and the degree of deuterium incorporation into each peptide is quantitated using MS, providing insights into the dynamics of individual protein sub-domains.

Overall, hCLIC5-WT exhibits a characteristic deuterium uptake distribution, in which secondary structure elements and the protein core show relatively low HDX levels, in contrast to the unstructured and peripheral regions, which show higher HDX levels (Figure 5). Importantly, the uptake of the TRX domain is on average higher than the α domain, throughout the time points sampled, highlighting the inherent flexibility of this fold (Figure 5A). With similar HDX levels as the inter-domain intervening linker, helix α2 of the TRX domain, together with helices α3, α4, and the N-terminal half of α5 of the α domain, demonstrate high HDX, suggesting they form

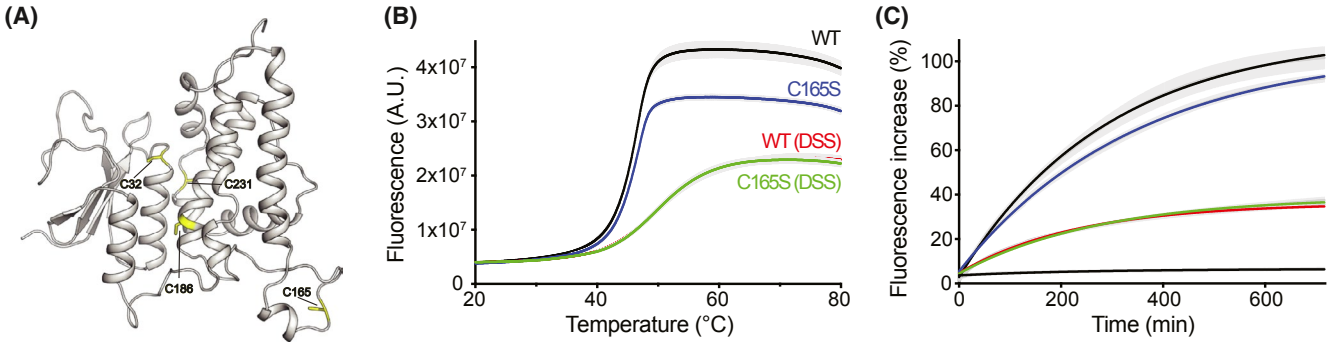

FIGURE 4 Inter-domain interface exposure inhibition by DSS. A, Cartoon representation of hCLIC5 highlighting the four endogenous cysteine residues (yellow). B, BFC-mediate cysteine accessibility analysis. Fluorescence-temperature relations of hCLIC5-WT and -C165S, in the presence or absence of preincubation with 1 mmol/L DSS, are presented. C, Cysteine accessibility kinetic analysis using BFC. Experimental groups are colored as in (B)

together a hinge mechanism allowing the opening of the inter-domain interface (Figure 5B). Conversely, the involvement of the α1 helix (P33-K45) in forming the inter-domain interface, via a three-helix bundle together with helices α2 and α6, is reflected by its lower HDX levels compared with the rest of the TRX domain (Figure 5B). Finally, helices α7 and α8, flanking the α domain opposite to the α3-α4 helices, show the lowest HDX levels, indicating high rigidity (Figure 5B). C165S exhibit a highly similar HDX profile as hCLIC5-WT, with high peripheral uptake levels and differential HDX between the TRX and α domains. Furthermore, even at the "foot loop" region, where C165 is localized, the mutation does not induce significant structural perturbation. Overall, the C165S mutation does not confer major conformational differences.

Next, we sought to identify residues which directly undergo modification following exposure to varying concentrations of H_2O_2 (Figure 6A). In line with the SEC-MALS characterization of oligomerization in solution (Figure 1B), ESI-MS analysis demonstrated that oxidation-mediated dimerization is completely abolished by the C165S mutant (Figure S5). Instead, these data uncovered that either monomeric hCLIC5-WT (see materials and methods section) or hCLIC5-C165S display an intriguing concentration-dependent mass shift, corresponding to the addition of dioxidation (Figure 6A). To pinpoint the modified residue, the proteins were digested, and the resulting peptides were subjected to LC-MS/MS. This analysis revealed that besides the dimer formation in WT, the only covalent modification induced by exposure to H_2O_2 is dioxidation of the highly conserved C32 to sulfinic acid (SO_2H) (Figure 6).

To segregate the effect of oxidation on the dynamics of monomeric hCLIC5 from the effects of oligomerization, we further assessed the response of hCLIC5-C165S to oxidative environment using HDX-MS (Figure 6B,C; Figure S7). Remarkably, following incubation with H_2O_2 a concentration-dependent increase in the exposure of specific interfacial constituents is observed. Specifically, the deuterium uptake is increased at the α1 helix, involved in the formation of the three-helix bundle, and the opposing highly protected α8. Thus, oxidative conditions modify the exposure level of the inter-domain interface. Together, the HDX profiles are consistent with our EOM analysis and site-directed covalent labeling with BFC, revealing a three-helix bundle at the core of the inter-domain interface and a hinge centered at the inter-domain linker, involving the flanking helices.

4 | DISCUSSION

Chloride intracellular channels were suggested to belong to a small but growing number of "metamorphic" proteins, which can adopt different folded conformations for the same amino acid sequence in native conditions.[55] While only CLIC1 was unequivocally shown to exhibit two distinct stable folds in solution,[24] all CLICs are thought to be present in cells both in soluble and integral membrane forms. However, while the transition between the two forms has centered considerable attention over the past decades, a holistic view of this process still awaits. The goal of the present study was to dissect the sequence of events enabling the transition of the

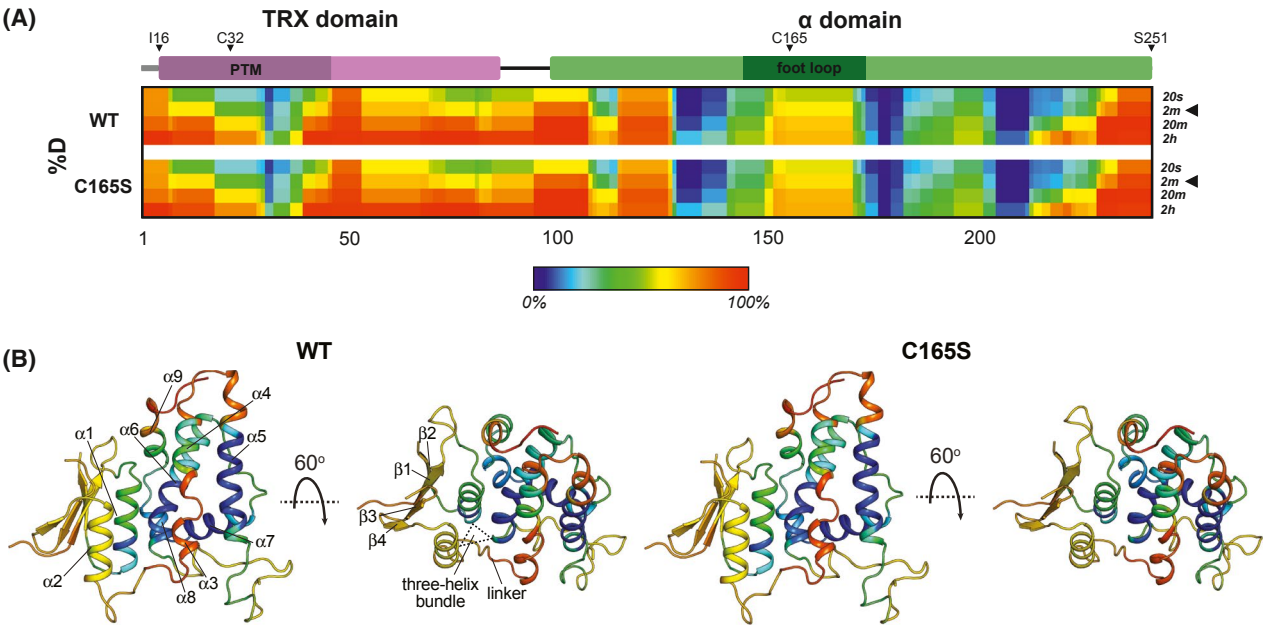

FIGURE 5 HDX profile analysis of hCLIC5. A, Rainbow heat maps of hCLIC5-WT and -C165S, ranging from 0% to 100% deuterium exchange at the indicated incubation periods. B, Cartoon representations of hCLIC5-WT and -C165S, colored according to (A). Indicated are secondary structure elements, the inter-domain linker region and the three-helix bundle (α1, α2, and α6)

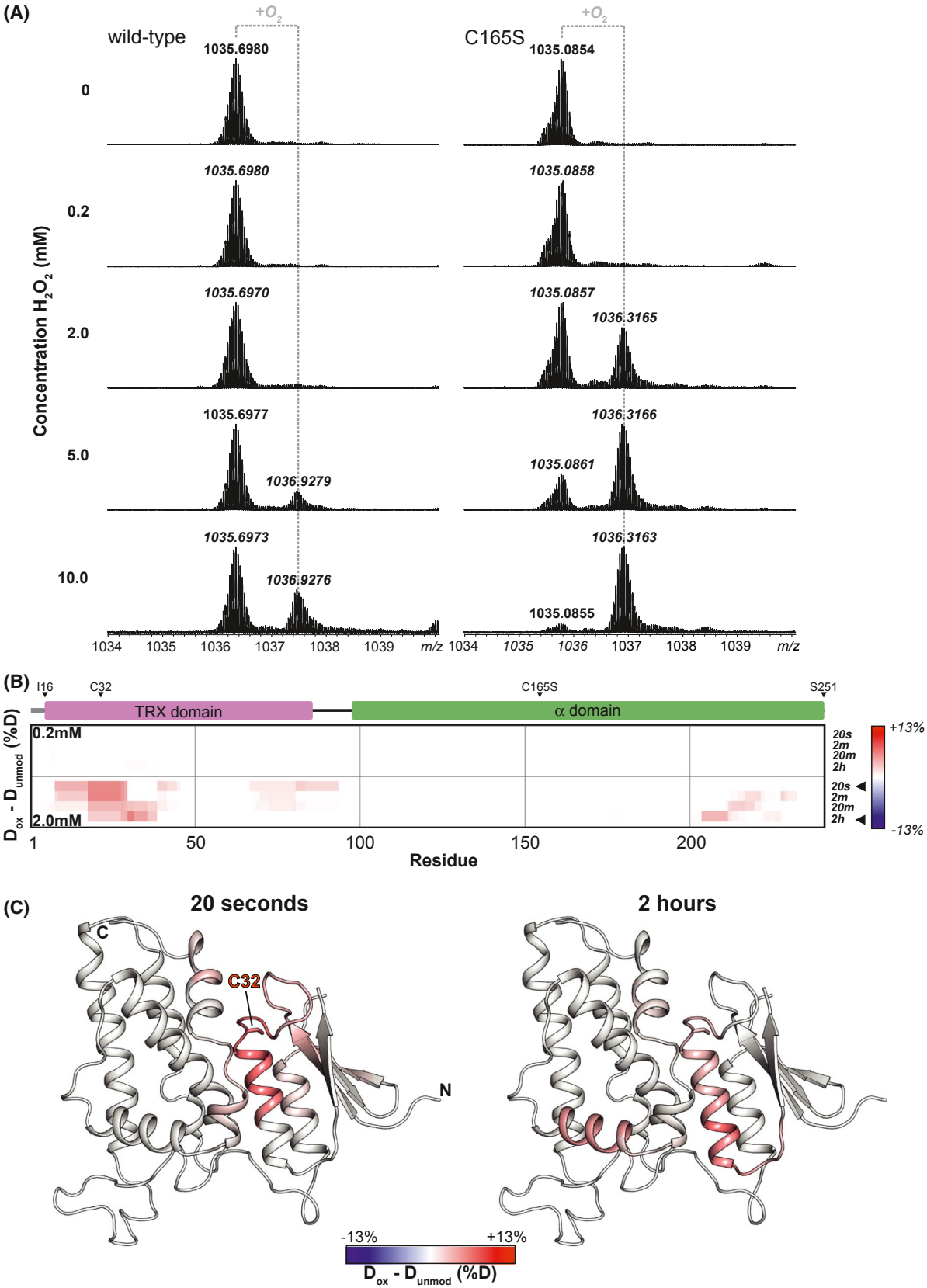

FIGURE 6 H_2O_2-mediated dioxidation of C32 is involved in the exposure of the inter-domain interface. A, Direct ESI-FT-ICR MS analysis of intact hCLIC5-WT (left) and -C165S (right) following incubation with increasing concentrations of H_2O_2 and treatment with 10 mmol/L TCEP. Detailed 26 + charge state is shown. Unoxidized and H_2O_2 oxidized forms were analyzed. B, Heat map summarizing differential HDX-MS analyses of unoxidized and oxidized forms of hCLIC5-C165S, following incubation with either 0.2 or 2 mmol/L H_2O_2. C, Cartoon representations of hCLIC5 colored as in (B) following incubation with 2 mmol/L H_2O_2 at the indicated time points. Data are presented as % deuterium difference

soluble monomeric hCLIC5 to a membrane interacting protein complex.

The partitioning of a protein between the aqueous and lipidic environments requires the conformational transition exposing hydrophobic protein sub-domains which favor interaction with the membrane. In CLIC1 an extensive oxidation-mediated conformational change leads to the exposure of a large hydrophobic interface. This structural transition was suggested to promote two competing processes.[55] That is, protein metamorphosis can promote either interaction with the membrane or protein dimerization. Nevertheless, the cysteine pair which mediate interface formation in CLIC1 is unique, leaving the general mechanisms involved in membrane interaction of CLIC family members ambiguous. Previously, we suggested that exposure of the inter-domain interface in CLIC6 plays a role in the membrane association process.[8] Importantly, this interface is highly conserved among CLIC family members (Figure 3B, Figure S1). Here, we studied hCLIC5 to determine whether the involvement of the inter-domain interface can be generalized.

Similar to CLIC1, hCLIC5 is able to dimerize in solution, via disulfide bridge formation (Figure 1). This finding was surprising since one of the cysteines involved in the intra-molecular disulfide bridge formation in CLIC1 is missing in hCLIC5. However, in contrast to CLIC1, systematic substitution of hCLIC5 cysteine residues revealed that dimers are formed by a distinct mechanism that involves a specific intermolecular disulfide bridge formation through C165 (Figure 1B). One may hypothesize that the oligomerization step is a common and crucial step in membrane interaction. Therefore, we pursued this notion using cross-linking and tryptophan fluorescence approaches, and demonstrated that oligomerization is not required for, and does not facilitate, the interaction with the membrane (Figure 2). Indeed, the C165S mutant revealed that the formation of higher oligomeric species in solution is not a prerequisite for oxidation-mediated oligomerization in the presence of membranes (Figure 2B).

Our results suggest that monomeric hCLIC5 can directly interact with membranes, and that this interaction is merely facilitated by oxidative environment (Figure 2D). Importantly, a similar mode of spontaneous interaction was also shown in CLIC1.[22] Therefore, we explored the structural properties of monomeric hCLIC5. The high-resolution crystal structure revealed that hCLIC5 shares high structural conservation with other CLIC family members, adopting a compact conformation (Figure 3A). Next, using SAXS, we explored the conformational landscape of hCLIC5-WT and hCLIC-C165S in solution. Similar to CLIC6,[8] both proteins exhibit a bimodal conformational distribution, with the majority occupying the compact form crystallized and the minority sampling an elongated conformation, likely exposing the hydrophobic inter-domain interface (Figure 3D). Indeed, site-directed covalent labeling with BFC corroborated the exposure of the inter-domain interface (Figure 4B,C). These analyses highlight the inherent flexibility of CLICs and hint toward a possible mechanism consisting of membrane interaction upon spontaneous exposure of the conserved inter-domain hydrophobic surface.

Nevertheless, if the interaction of hCLIC5 can rely on a purely spontaneous mechanism, what is the mechanism for oxidation-facilitated membrane interaction? We hypothesized that oxidative environment may increase the exposure of the hydrophobic interface to the bulk solution. First, we used HDX-MS and showed that the deuterium uptake profiles of hCLIC5-WT and C165S are essentially identical and are consistent with the exposure of the inter-domain interface, as suggested by the SAXS analysis (Figure 5). To pinpoint the dynamic changes imposed by oxidation, we first identified modified residues upon exposure to H_2O_2. MS analyses revealed an oxidation of C32, which lies at the inter-domain interface and forms part of the strictly conserved C-P-(F/S)-(S/C) glutaredoxin-like site, known to covalently interact with glutathione (Figure 6A, Figure S1). Interestingly, CLIC1 C24, the position corresponding to C32 in hCLIC5, was previously suggested to constitute a redox-sensitive residue, positioned on the extracellular side following membrane insertion, and to participate in channel regulation.[56] Next, to characterize the effect of oxidation on monomeric hCLIC5, we resorted to the use of HDX-MS, comparing oxidized versus naïve hCLIC5-C165S. Strikingly, oxidation of hCLIC5 results in a specific and localized increase in deuterium uptake within the inter-domain interface, reflecting a less rigid conformation and increased bulk solvent exposure (Figure 6B,C). Thus, the HDX-MS results align with our initial hypothesis stating that oxidative environment facilitates hCLIC5 inter-domain reorientation in solution, leading to an increased propensity for membrane interaction.

Our results suggest that CLICs may undergo membrane insertion following a mechanism reminiscent of that described for pore-forming toxins, such as lysenin.[57] Secreted as a soluble monomer, this member of the aerolysin family exists as a monomer in solution. Upon exposure to sphingomyelin (SM)-containing membranes, lysenin undergoes a sequence of structural transitions, from water-soluble monomers into a membrane-embedded lytic β-barrel pore. First, lysenin monomers attach to the membrane surface via SM molecules. Next, the attachment to the SM-rich membrane domains facilitates the formation of an oligomeric pre-pore complex. Finally, a large conformational rearrangement leads to membrane insertion and pore formation. Similarly, we propose the following mechanism for CLICs. Specifically, in their compact conformation, globular CLICs localize to the cytosol. A small fraction

(~10%) of the protein exhibits an elongated conformation, which favors membrane interaction. Following exposure to an oxidative environment, the inter-domain interface is destabilized, skewing the conformational distribution toward the elongated conformation, thereby enhancing membrane interaction. Next, oligomers are formed at the membrane, ultimately resulting in pore formation. In support with this proposed general mechanism, the membrane insertion process of CLIC1 was previously shown to depend on the presence of cholesterol,[58] similar the cholesterol-dependent-cytolysin family of bacterial pore-forming proteins.

In conclusion, we propose that the ability of CLICs to interact with the membrane is an intrinsic property, predefined by their conformational landscape and specifically, exposure of the conserved hydrophobic inter-domain interface. Moreover, oligomerization in solution is not a prerequisite for pore formation and an oxidative environment is a mere facilitator of structural transitions underlying membrane association.

5 | ACCESSION NUMBER

Atomic coordinates and structure factors have been deposited in the Protein Data Bank with accession number 6Y2H.

ACKNOWLEDGMENTS

We thank the staff of beamlines ID30B and BM29 at the ESRF for assistance with diffraction experimentation. We also thank Dr. Moran Rubinstein and members of the Haitin lab for advice and support. This work was performed in partial fulfillment of the requirements for a PhD degree of AF, Sackler Faculty of Medicine, Tel Aviv University, Israel. This work was supported by the Israel Science Foundation grant 1721/16 (YH) Israel Cancer Research Foundation grants 01214 (YH) and 19202 (MG), and the German-Israeli Foundation for Scientific Research and Development (GIF) grant I-2425-418.13/2016 (YH). Support also came from the I-CORE Program of the Planning and Budgeting Committee and The Israel Science Foundation grant 1775/12 (YH). Access to an EU_FT–ICR_MS network installation was funded by the EU Horizon 2020 grant 731077. Additional support from CSF (19-16084S) and MEYS CZ Funds (CZ.1.05/1.1.00/02.0109 and LM2015043) is gratefully acknowledged.

AUTHOR CONTRIBUTIONS

Conceived and designed the experiments: Alisa Ferofontov, Moshe Giladi, and Yoni Haitin. Performed the experiments: Alisa Ferofontov and Pavla Vankova. Analyzed the data: Alisa Ferofontov, Pavla Vankova, Petr Man, and Moshe Giladi. Wrote the paper: Alisa Ferofontov, Moshe Giladi, and Yoni Haitin.

REFERENCES

1. ArgenzioE, Moolenaar WH. Emerging biological roles of Cl^- intracellular channel proteins. *J Cell Sci*. 2016;129.
2. LandryDW, Akabas MH, Redhead C, Edelman A, Cragoe EJ, Al-Awqati Q. Purification and reconstitution of chloride channels from kidney and trachea. *Science*. 1989;244:1469-1472.
3. DulhuntyA, Gage P, Curtis S, Chelvanayagam G, Board P. The glutathione transferase structural family includes a nuclear chloride channel and a ryanodine receptor calcium release channel modulator. *J Biol Chem*. 2001;276:3319-3323.
4. HarropSJ, DeMaere MZ, Fairlie WD, et al. Crystal structure of a soluble form of the intracellular chloride ion channel CLIC1 (NCC27) at 1.4-Å resolution. *J Biol Chem*. 2001;276:44993-45000.
5. CromerBA, Gorman MA, Hansen G, et al. Structure of the janus protein human CLIC2. *J Mol Biol*. 2007;374:719-731.
6. LittlerDR, Brown LJ, Breit SN, Perrakis A, Curmi PMG. Structure of human CLIC3 at 2 Å resolution. *Proteins Struct Funct Bioinforma*. 2010;78:1594-1600.
7. LittlerDR, Assaad NN, Harrop SJ, et al. Crystal structure of the soluble form of the redox-regulated chloride ion channel protein CLIC4. *FEBS J*. 2005;272:4996-5007.
8. FerofontovA, Strulovich R, Marom M, Giladi M, Haitin Y. Inherent flexibility of CLIC6 revealed by crystallographic and solution studies. *Sci Rep*. 2018;8:6882.
9. LittlerDR, Harrop SJ, Brown LJ, et al. Comparison of vertebrate and invertebrate CLIC proteins: the crystal structures of Caenorhabditis elegans EXC-4 and Drosophila melanogaster DmCLIC. *Proteins*. 2008;71:364-378.
10. LittlerDR, Harrop SJ, Goodchild SC, et al. The enigma of the CLIC proteins: Ion channels, redox proteins, enzymes, scaffolding proteins? *FEBS Lett*. 2010;584:2093-2101.
11. CarofinoBL, Dinshaw KM, Ho PY, et al. Head and neck squamous cancer progression is marked by CLIC4 attenuation in tumor epithelium and reciprocal stromal upregulation of miR-142-3p, a novel post-transcriptional regulator of CLIC4. *Oncotarget*. 2019;10:7251-7275.
12. SuhKS, Mutoh M, Gerdes M, Yuspa SH. CLIC4, an intracellular chloride channel protein, is a novel molecular target for cancer therapy. *J Investig Dermatol Symp Proc*. 2005;10:105-109.
13. Hernandez-FernaudJR, Ruengeler E, Casazza A, et al. Secreted CLIC3 drives cancer progression through its glutathione-dependent oxidoreductase activity. *Nat Commun*. 2017;8:14206.
14. CarliniV, Verduci I, Cianci F, et al. CLIC1 protein accumulates in circulating monocyte membrane during neurodegeneration. *Int J Mol Sci*. 2020;21(4):1484.
15. JiaN, Dong S, Zhao G, Gao H, Li X, Zhang H. CLIC1 overexpression is associated with poor prognosis in pancreatic ductal adenocarcinomas. *J Cancer Res Ther*. 2016;12:892-896.
16. SinghaB, Harper SL, Goldman AR, et al. CLIC1 and CLIC4 complement CA125 as a diagnostic biomarker panel for all subtypes of epithelial ovarian cancer. *Sci Rep*. 2018;8:14725.
17. WithamS, Takano K, Schwartz C, Alexov E. A missense mutation in CLIC2 associated with intellectual disability is predicted by in silico modeling to affect protein stability and dynamics. *Proteins Struct Funct Bioinforma*. 2011;79:2444-2454.
18. Gururaja RaoS, Patel NJ, Singh H. Intracellular chloride channels: novel biomarkers in diseases. *Front Physiol*. 2020;11:96.

19. TakanoK, Liu D, Tarpey P, et al. An x-linked channelopathy with cardiomegaly due to a CLIC2 mutation enhancing ryanodine receptor channel activity. *Hum Mol Genet*. 2012;21:4497-4507.
20. PatelSH, Edwards MJ, Ahmad SA. Intracellular ion channels in pancreas cancer. *Cell Physiol Biochem*. 2019;53:44-51.
21. PerettiM, Angelini M, Savalli N, Florio T, Yuspa SH, Mazzanti M. Chloride channels in cancer: Focus on chloride intracellular channel 1 and 4 (CLIC1 AND CLIC4) proteins in tumor development and as novel therapeutic targets. *Biochim Biophys Acta*. 2015;1848:2523-2531.
22. GoodchildSC, Howell MW, Cordina NM, et al. Oxidation promotes insertion of the CLIC1 chloride intracellular channel into the membrane. *Eur Biophys J*. 2009;39:129-138.
23. StoychevSH, Nathaniel C, Fanucchi S, et al. Structural dynamics of soluble chloride intracellular channel protein CLIC1 examined by amide hydrogen-deuterium exchange mass spectrometry. *Biochemistry*. 2009;48:8413-8421.
24. LittlerDR, Harrop SJ, Fairlie WD, et al. The intracellular chloride ion channel protein CLIC1 undergoes a redox-controlled structural transition. *J Biol Chem*. 2004;279:9298-9305.
25. HossainKR, Turkewitz DR, Holt SA, et al. A conserved GXXXG motif in the transmembrane domain of CLIC proteins is essential for their cholesterol-dependant membrane interaction. *Biochim Biophys Acta Gen Subj* 2019;1863:1243-1253.
26. GagnonLH, Longo-Guess CM, Berryman M, et al. The chloride intracellular channel protein CLIC5 is expressed at high levels in hair cell stereocilia and is essential for normal inner ear function. *J Neurosci*. 2006;26:10188-10198.
27. SecoCZ, Oonk AMM, Domínguez-Ruiz M, et al. Progressive hearing loss and vestibular dysfunction caused by a homozygous nonsense mutation in CLIC5. *Eur J Hum Genet*. 2015;23:189-194.
28. NeveuB, Spinella JF, Richer C, et al. CLIC5: A novel ETV6 target gene in childhood acute lymphoblastic leukemia. *Haematologica*. 2016;101:1534-1543.
29. BamfordS, Dawson E, Forbes S, et al. The COSMIC (Catalogue of Somatic Mutations in Cancer) database and website. *Br J Cancer*. 2004;91:355-358.
30. Collaborative Computational Project, N. 4. The CCP4 suite: Programs for protein crystallography. *Acta Crystallogr Sect D Biol Crystallogr*. 1994;50:760-763.
31. StrongM, Sawaya MR, Wang S, Phillips M, Cascio D, Eisenberg D. Toward the structural genomics of complexes: crystal structure of a PE/PPE protein complex from Mycobacterium tuberculosis. *Proc Natl Acad Sci USA*. 2006;103:8060-8065.
32. McCoyAJ. Solving structures of protein complexes by molecular replacement with Phaser. *Acta Crystallogr Sect D Biol Crystallogr*. 2006;63:32-41.
33. AdamsPD, Afonine PV, Bunkóczi G, et al. PHENIX: A comprehensive Python-based system for macromolecular structure solution. *Acta Crystallogr Sect D Biol Crystallogr*. 2010;66:213-221.
34. EmsleyP, Cowtan K. Coot: Model-building tools for molecular graphics. *Acta Crystallogr Sect D Biol Crystallogr*. 2004;60:2126-2132.
35. KochMHJ, Vachette P, Svergun DI. Small-angle scattering: A view on the properties, structures and structural changes of biological macromolecules in solution. *Q Rev Biophys*. 2003;36:147-227.
36. KonarevPV, Volkov VV, Sokolova AV, Koch MHJ, Svergun DI. PRIMUS: a Windows PC-based system for small-angle scattering data analysis. *J Appl Crystallogr*. 2003;36:1277-1282.
37. PetoukhovMV, Franke D, Shkumatov AV, et al. New developments in the ATSAS program package for small-angle scattering data analysis. *J Appl Crystallogr*. 2012;45:342-350.
38. SvergunD, Barberato C, Koch MH. CRYSOL - A program to evaluate X-ray solution scattering of biological macromolecules from atomic coordinates. *J Appl Crystallogr*. 1995;28:768-773.
39. EswarN, Eramian D, Webb B, Shen M-Y, Sali A. Protein structure modeling with MODELLER. *Methods Mol Biol Then Totowa*. 2008;426:145.
40. BernadóP, Mylonas E, Petoukhov MV, Blackledge M, Svergun DI. Structural characterization of flexible proteins using small-angle X-ray scattering. *J Am Chem Soc*. 2007;129:5656-5664.
41. HofmannL, Gulati S, Sears A, Stewart PL, Palczewski K. An effective thiol-reactive probe for differential scanning fluorimetry with a standard real-time polymerase chain reaction device. *Anal Biochem*. 2016;499:63-65.
42. TrckaF, Durech M, Vankova P, et al. Human stress-inducible Hsp70 has a high propensity to form ATP-dependent antiparallel dimers that are differentially regulated by cochaperone binding. *Mol Cell Proteomics*. 2019;18:320-337.
43. ZhangZ, Smith DL. Determination of amide hydrogen exchange by mass spectrometry: a new tool for protein structure elucidation. *Protein Sci*. 1993;2:522-531.
44. KavanD, Man P. MSTools - Web based application for visualization and presentation of HXMS data. *Int J Mass Spectrom*. 2011;302:53-58.
45. FilandrF, Kavan D, Kracher D, et al. Structural dynamics of lytic polysaccharide monooxygenase during catalysis. *Biomolecules*. 2020;10:242.
46. GoodchildSC, Angstmann CN, Breit SN, Curmi PMG, Brown LJ. Transmembrane extension and oligomerization of the CLIC1 chloride intracellular channel protein upon membrane interaction. *Biochemistry*. 2011;50:10887-10897.
47. Al KhamiciH, Hossain KRK, Cornell BA, Valenzuela SM. Investigating sterol and redox regulation of the ion channel activity of CLIC1 using tethered bilayer membranes. *Membranes (Basel)*. 2016;6:51.
48. VivianJT, Callis PR. Mechanisms of tryptophan fluorescence shifts in proteins. *Biophys J*. 2001;80:2093-2109.
49. LandryD, Sullivan S, Nicolaides M, et al. Molecular cloning and characterization of p64, a chloride channel protein from kidney microsomes. *J Biol Chem*. 1993;268:14948-14955.
50. ValenzuelaSM, Martin DK, Por SB, et al. Molecular cloning and expression of a chloride ion channel of cell nuclei. *J Biol Chem*. 1997;272:12575-12582.
51. AshkenazyH, Abadi S, Martz E, et al. ConSurf 2016: an improved methodology to estimate and visualize evolutionary conservation in macromolecules. *Nucleic Acids Res*. 2016;44:W344-W350.
52. GoodchildSC, Howell MW, Littler DR, et al. Metamorphic response of the CLIC1 chloride intracellular ion channel protein upon membrane interaction. *Biochemistry*. 2010;49:5278-5289.
53. PotrzebowskiW, Trewhella J, Andre I. Bayesian inference of protein conformational ensembles from limited structural data. *PLOS Comput Biol*. 2018;14:e1006641.
54. KonermannL, Pan J, Liu YH. Hydrogen exchange mass spectrometry for studying protein structure and dynamics. *Chem Soc Rev*. 2011;40:1224-1234.

55. GoodchildSC, Curmi PMG, Brown LJ. Structural gymnastics of multifunctional metamorphic proteins. *Biophys Rev*. 2011;3:143-153.
56. SinghH, Ashley RH. Redox regulation of CLIC1 by cysteine residues associated with the putative channel pore. *Biophys J*. 2006;90:1628-1638.
57. KulmaM, Dadlez M, Kwiatkowska K. Insight into the structural dynamics of the Lysenin during prepore-to-pore transition using hydrogen–deuterium exchange mass spectrometry. *Toxins (Basel)*. 2019;11:462.
58. ValenzuelaSM, Alkhamici H, Brown LJ, et al. Regulation of the membrane insertion and conductance activity of the metamorphic chloride intracellular channel protein CLIC1 by cholesterol. *PLoS ONE*. 2013;8:e56948.

SUPPORTING INFORMATION

Additional Supporting Information may be found online in the Supporting Information section.

How to cite this article: Ferofontov A, Vankova P, Man P, Giladi M, Haitin Y. Conserved cysteine dioxidation enhances membrane interaction of human Cl^- intracellular channel 5. *The FASEB Journal*. 2020;34:9925–9940. https://doi.org/10.1096/fj.202000399R